Aruna *et al. Journal of Cardiothoracic Surgery* (2026) 21:581
https://doi.org/10.1186/s13019-026-04362-9

Journal of Cardiothoracic Surgery

RESEARCH Open Access

Network pharmacology and experimental evaluation of Sanwei Tanxiang Tangsan in doxorubicin-induced heart failure

Aruna[1†], Dulan[1†], Davaadagva Damdinjav[2], Battulga Tungalag[2], GuiZhi[1] and Hua Li[1*]

Abstract

Background Heart failure (HF) is a complex syndrome characterized by inflammation, oxidative stress, and cardiomyocyte apoptosis, for which effective and well-tolerated therapies remain limited. This study sought to explore the potential mechanisms by which Mongolian medicine Sanwei Tanxiang Tangsan (STX) may be associated with AKT1/p53-related signaling in the mitigation of HF, employing network pharmacology, molecular docking, and animal experimentation.

Materials and methods Active constituents and corresponding targets of Mongolian medicine STX were systematically screened, followed by the construction of drug–disease interaction networks to identify pivotal proteins and pathways. A doxorubicin-induced HF rat model was established, and after four weeks of intragastric administration of Mongolian medicine STX and sacubitril/valsartan (angiotensin receptor–neprilysin inhibitor, positive control), cardiac functional parameters and expression levels of AKT protein 1 (AKT1), interleukin-6 (IL-6), and p53 were assessed.

Result Nineteen active components were identified in Mongolian medicine STX, interacting with 153 HF-associated targets, among which AKT1, IL-6, and TP53 served as the core genes. Molecular docking analysis revealed that quercetin and luteolin possessed moderate predicted binding affinities and stable interactions with the corresponding targets. Animal experiments indicated that Mongolian medicine STX significantly reduced N-terminal pro-brain natriuretic peptide levels and altered myocardial AKT1, IL-6, and p53 protein abundance. However, echocardiographic parameters showed no statistically significant improvement compared with the Model group.

Conclusion Mongolian medicine STX may exert cardioprotective effects in HF, as reflected by improvements in biochemical and histopathological indicators, and these effects may be associated with AKT1/p53-related signaling pathways. However, direct pathway activation and causal mechanisms were not confirmed in the present study and require further investigation.

Keywords AKT1/p53 pathway, Animal experiments, Heart failure, Network pharmacology, Sanwei Tanxiang Tangsan

[†]Aruna and Dulan contributed equally to this work and share first authorship.

*Correspondence:
Hua Li
hua-li@ldy.edu.rs

[1]Inner Mongolia Medical University, Hohhot City 010110, Inner Mongolia Autonomous Region, China
[2]Mongolian National University of Medical Sciences, Ulaanbaatar 999097, Mongolia

© The Author(s) 2026, modified publication 2026. **Open Access** This article is licensed under a Creative Commons Attribution 4.0 International License, which permits use, sharing, adaptation, distribution and reproduction in any medium or format, as long as you give appropriate credit to the original author(s) and the source, provide a link to the Creative Commons licence, and indicate if changes were made. The images or other third party material in this article are included in the article's Creative Commons licence, unless indicated otherwise in a credit line to the material. If material is not included in the article's Creative Commons licence and your intended use is not permitted by statutory regulation or exceeds the permitted use, you will need to obtain permission directly from the copyright holder. To view a copy of this licence, visit http://creativecommons.org/licenses/by/4.0/.

Introduction

As the terminal manifestation of cardiovascular disorders, heart failure (HF) continues to pose a formidable challenge in global cardiovascular medicine owing to its unfavorable clinical prognosis. Recent clinical guidelines have indicated that angiotensin receptor–neprilysin inhibitors (ARNI), sodium-glucose cotransporter 2 inhibitors, and other pharmacological agents have been verified to exert definitive therapeutic benefits for HF [1]. Nevertheless, their clinical utility remains constrained by adverse effects such as cough and hyperkalemia [2]. Therefore, the development of therapeutic strategies with pronounced efficacy and improved safety profiles remains an essential objective within contemporary HF research. The pathological mechanisms underlying HF are multifaceted, predominantly encompassing biological processes such as inflammatory response, oxidative stress, and apoptosis [3]. Previous investigations conducted by the research group have suggested that the AKT1/P53 pathway may function as an important regulatory axis in the pathological progression of HF and maintains extensive crosstalk with multiple downstream signaling cascades, thereby representing a potential therapeutic target for HF. However, direct experimental validation of this pathway in the context of Mongolian medicine remains limited.

Within the theoretical framework of Mongolian medicine, HF is categorized as "cardiac edema", with therapeutic principles centered on promoting the circulation of qi and blood and restoring cardiac function [4]. The Mongolian medicine Sanwei Tanxiang Tangsan (STX) has been shown to possess potential therapeutic efficacy in the management of HF. This prescription comprises three medicinal components: *Santalum album*, *Choerospondias axillaris*, and *Myristica fragrans*. Previous investigations have demonstrated its capacity to enhance cardiac performance and suppress myocardial fibrosis [5]. Nevertheless, the precise molecular mechanisms responsible for its therapeutic effects against HF remain inadequately defined. In light of this, this study was designed to systematically explore the potential mechanisms underlying the anti-HF effects of Mongolian medicine STX, integrating approaches from network pharmacology and animal experimentation, with particular focus on its possible association with AKT1/p53-related signaling pathways rather than direct mechanistic confirmation.

Materials and methods

Drugs and reagents

Doxorubicin (Cat. No.: D1515, Sigma-Aldrich) was dissolved in physiological saline for intraperitoneal administration. Mongolian medicine STX was obtained from Inner Mongolia Mongolian Medicine Factory (National Drug Approval No. Z20027787), and ARNI (sacubitril/valsartan, 100 mg × 14 tablets, National Drug Approval No. 20170363) was procured from the Western Pharmacy of the Affiliated Hospital of Inner Mongolia Medical University. Both preparations were diluted to the required concentrations using double-distilled water before use. The rat N-terminal pro-brain natriuretic peptide (NT-proBNP) ELISA kit was procured from Jiangsu Enzyme-linked Biotechnology Co., Ltd. (Cat. No.: MM-0329R1); the rat AKT protein 1 (AKT1) ELISA kit was obtained from the same company (Cat. No.: MM-72018R2); the rat interleukin-6 (IL-6) ELISA kit (Cat. No.: MM-0190R2) and rat p53 (p53) ELISA kit (Cat. No.: MM-61460R2) were also sourced from Jiangsu Enzyme-linked Biotechnology Co., Ltd. The Masson staining kit was supplied by Beijing Solarbio Science & Technology Co., Ltd. (Cat. No.: G1340-7). All ELISA kits were used strictly according to the manufacturers' instructions, and the assays were performed in duplicate to ensure reproducibility.

Experimental animals

Thirty-two specific pathogen-free male Sprague-Dawley rats, aged 6–8 weeks and weighing (220 ± 20) g, were obtained from Beijing Sibeifu Laboratory Animal Technology Co., Ltd. (Animal Production License No. SCXK (Jing) 2024-0001). The animals were maintained in the Laboratory Animal Center of Inner Mongolia Medical University under controlled environmental conditions, including a constant temperature of 25 °C, relative humidity of 55% ± 5%, and a 12 h/12 h light-dark cycle, with unrestricted access to standard chow and water. All experimental procedures involving animals were reviewed and approved by the Laboratory Animal Welfare and Ethics Committee of Inner Mongolia Medical University (Approval No. KYD20240386). All animal care and experimental protocols were conducted in strict accordance with the Guidelines for the Care and Use of Laboratory Animals (National Institutes of Health, USA) and the ARRIVE 2.0 reporting standards. At the end of the experiment, rats were euthanized under deep anesthesia using pentobarbital sodium (150 mg/kg, intraperitoneally), an internationally accepted and humane method for rodent euthanasia.

Collection and screening of chemical components of Mongolian medicine STX and prediction of target proteins

The Traditional Chinese Medicine Systems Pharmacology (TCMSP) database was employed to retrieve the chemical constituents of *Santalum album*, *Choerospondias axillaris*, and *Myristica fragrans*, respectively. Active compounds were screened according to oral bioavailability (≥ 30%) and drug-likeness (≥ 0.18) parameters to identify the effective constituents. Subsequently, the corresponding target protein sets for these constituents were obtained. The UniProt database was utilized under the

conditions of "Homo sapiens" and "reviewed" to retrieve the gene names associated with each target protein. After excluding targets lacking corresponding gene annotations and removing duplicates, the final gene set of Mongolian medicine STX was compiled.

Collection and screening of disease-related genes

The DisGeNET, GeneCards, Online Mendelian Inheritance in Man (OMIM), and Therapeutic Target Database (TTD) databases were employed to identify HF-related targets by using "heart failure" as the search keyword in each database. Targets retrieved from GeneCards were ranked according to relevance score, and three successive rounds of median-based filtering were applied to exclude low-relevance genes; however, this approach did not incorporate tissue-specific weighting and is acknowledged as a potential limitation.

Construction of drug component–disease target network

The gene set of Mongolian medicine STX and the HF target set were imported into Venny 2.1 to generate a Venn diagram, from which the intersecting genes were extracted. The resulting drug component–target gene dataset was subsequently imported into Cytoscape 3.7.1 software, where a type file containing the drug–disease intersecting genes was created and reimported. After the exclusion of genes unrelated to the disease, a "drug component–target–disease" network was constructed and optimized to further elucidate the associations between disease genes and drug components.

Construction of protein–protein interaction (PPI) network

The list of intersecting genes was entered into the STRING database with the organism restricted to "Homo sapiens". The confidence score threshold was set at ≥ 0.4, and isolated targets were excluded to generate the PPI network. The resulting network map and tab-separated values (TSV) file were subsequently exported. The TSV file was then imported into Cytoscape 3.7.1 software, where core genes were identified according to "degree" values and subjected to visualization for analytical interpretation.

Gene enrichment analysis

In the Database for Annotation, Visualization and Integrated Discovery (DAVID), the gene identifier was set to OFFICIAL_GENE_SYMBOL, and the organism was restricted to Homo sapiens to obtain information in three categories: biological process (BP), cellular component (CC), and molecular function (MF), along with Kyoto Encyclopedia of Genes and Genomes (KEGG) pathway data. Subsequently, bar plots for Gene Ontology (GO) enrichment analysis and bubble plots for KEGG pathway annotation were generated using the Weishengxin platform.

Molecular docking

Molecular docking was conducted between the screened core components of the drug and their corresponding core targets. The 3D structures of the principal active compounds were obtained from the TCMSP database, while the core target proteins in PDB format were retrieved from the PDB database. The prepared data were subsequently imported into AutoDockTools 1.5.6 for docking simulations, and PyMOL 3.1.0 software was employed for macromolecular preprocessing and visualization of the docking results. Docking simulations were performed using AutoDockTools 1.5.6, and binding affinities were evaluated based on the predicted binding energy values, with lower values indicating stronger predicted interactions.

Experimental animal treatment protocol

After a one-week acclimatization period, the rats were randomly allocated to the control (Con) group ($n = 8$) and the model (Mod) group ($n = 24$). The Mod group received intraperitoneal injections of doxorubicin once per week, administered at a dosage of 3 mg/kg for the initial three weeks and 2 mg/kg for the subsequent three weeks. The Con group was given an equivalent volume of normal saline through intraperitoneal injection. Upon successful establishment of the Mod model, the 24 rats were randomly assigned to the Mod group, Western medicine group (ARNI, 18 mg/kg), and Mongolian medicine group (STX, 0.54 g/kg), each receiving its respective treatment ($n = 8$ per group) once daily. The Con and Mod groups were administered an equivalent volume of double-distilled water by gavage. After four weeks of treatment, rats in all groups were sacrificed, and biological samples were subsequently collected. The STX dose (0.54 g/kg/day) was selected based on conversion from the clinical dosage and previous experimental studies.

Cardiac function assessment

NT-proBNP levels were determined using an NT-proBNP assay kit to assess the severity of HF in rats, and echocardiographic evaluation was subsequently conducted. Detection of AKT1, IL6, and TP53 protein levels in myocardial tissue by ELISA.

The myocardial protein levels of AKT1, IL6, and TP53 were quantified using the enzyme-linked immunosorbent assay (ELISA) technique. Briefly, myocardial tissues were homogenized in ice-cold phosphate-buffered saline, centrifuged to obtain supernatants, and total protein concentrations were normalized prior to ELISA measurement. ELISA detects total protein abundance and does

not reflect phosphorylation-dependent activation of signaling pathways.

Statistical analysis

Statistical analyses were conducted using SPSS Statistics 27.0 software, while graphical representations were generated with GraphPad Prism 9.5.1 software. Measurement data were denoted as mean ± standard deviation (x ± s). One-way analysis of variance (ANOVA) was utilized for comparisons among multiple groups, followed by Tukey's post-hoc test for multiple comparisons, with $P < 0.05$ indicating statistical significance.

Table 1 Active ingredients of Sanwei Tanxiang Tangsan

Mongolian medicine	Mol ID	Molecule name	OB (%)	DL	Code
Santalum album	MOL000354	Isorhamnetin	49.6	0.31	TX1
	MOL000006	Luteolin	36.16	0.25	TX2
	MOL002322	Isovitexin	31.29	0.72	TX3
Choerospondias axillaris	MOL001002	Ellagic acid	43.06	0.43	GZ1
	MOL001040	(2R)−5,7-Dihydroxy-2-(4-hydroxyphenyl) chroman-4-one	42.36	0.21	GZ2
	MOL001490	Bis[(2 S)−2-ethylhexyl] benzene-1,2-dicarboxylate	43.59	0.35	GZ3
	MOL001736	(-)-Taxifolin	60.51	0.27	GZ4
	MOL000358	β-Sitosterol	36.91	0.75	A
	MOL000422	Kaempferol	41.88	0.24	GZ5
	MOL004328	Naringenin	59.29	0.21	GZ6
	MOL000096	(-)-Catechin	49.68	0.24	GZ7
	MOL000098	Quercetin	46.43	0.28	GZ8
Myristica fragrans	MOL000358	β-Sitosterol	36.91	0.75	A
	MOL007920	Meso-1,4-Bis-(4-hydroxy-3-methoxyphenyl)−2,3-dimethylbutane	31.32	0.26	—
	MOL009243	Isoguaiacin	48.78	0.31	RDK1
	MOL009254	Galbacin	61.00	0.53	RDK2
	MOL009255	5-[(2 S,3 S)−7-Methoxy-3-methyl-5-[(E)-prop-1-enyl]−2,3-dihydrobenzofuran-2-yl]−1,3-benzodioxole	53.11	0.40	RDK3
	MOL009259	Kudos	45.06	0.38	RDK4
	MOL009263	Saucernetindiol	41.85	0.32	RDK5
	MOL009264	Tetrahydrofuroguaiacin B	62.86	0.32	RDK6
	MOL009265	Threo-Austrobailignan-5	49.49	0.32	RDK7

Active components were screened based on oral bioavailability (OB ≥ 30%) and drug-likeness (DL ≥ 0.18) from the TCMSP database. β-sitosterol was identified as a shared component between Choerospondias axillaris and Myristica fragrans

Results

Collection of active components and target proteins of Mongolian medicine STX

Nineteen active components of Mongolian medicine STX were retrieved from the TCMSP database. Among these, *Santalum album* contained three components, *Choerospondias axillaris* included nine components, and *Myristica fragrans* comprised eight components. β-sitosterol was identified as the shared active constituent between *Choerospondias axillaris* and *Myristica fragrans*. The detailed information is summarized in Table 1. After further retrieval, screening, and deduplication, a total of 234 target genes associated with Mongolian medicine STX were ultimately obtained.

Identification of potential targets of Mongolian medicine STX for HF treatment

A total of 15,687 genes were retrieved from the GeneCards database, and 1,961 genes were retained after three successive rounds of median screening based on the "relevance score" criterion. The DisGeNET database yielded 1,499 genes, the OMIM database identified 619 genes, and the TTD database contributed 61 genes. By integrating the search outcomes from these four databases, a total of 3,343 HF-related targets were obtained. Subsequently, the gene set of Mongolian medicine STX and the HF target set were imported into Venny 2.1 software to construct a Venn diagram, from which 153 overlapping genes were identified. The overlap among databases is presented in Supplementary Figure S1.

Construction of drug component–disease target network diagram

The drug component–target gene dataset was imported into Cytoscape 3.7.1 software for visualization analysis (Fig. 1). Based on the degree value ranking, the top five active components were identified as quercetin, kaempferol, luteolin, β-sitosterol, and naringenin. These components were identified based on network topology and should be interpreted as candidate bioactive compounds rather than definitive therapeutic determinants.

Construction of PPI network

The intersecting gene list was imported into the STRING database for visualization analysis (Fig. 2A). The ten target genes with the highest degree values were AKT1, TNF, IL6, IL1B, TP53, PTGS2, CASP3, JUN, ESR1, and EGFR. Among these, the core genes AKT1, TNF, IL6, IL1B, and P53 were identified as hub genes within the interaction network involved in the onset, progression, and pharmacological modulation of HF, with AKT1 identified as the most significant protein (Fig. 2B). However, these hub genes are commonly observed in multiple

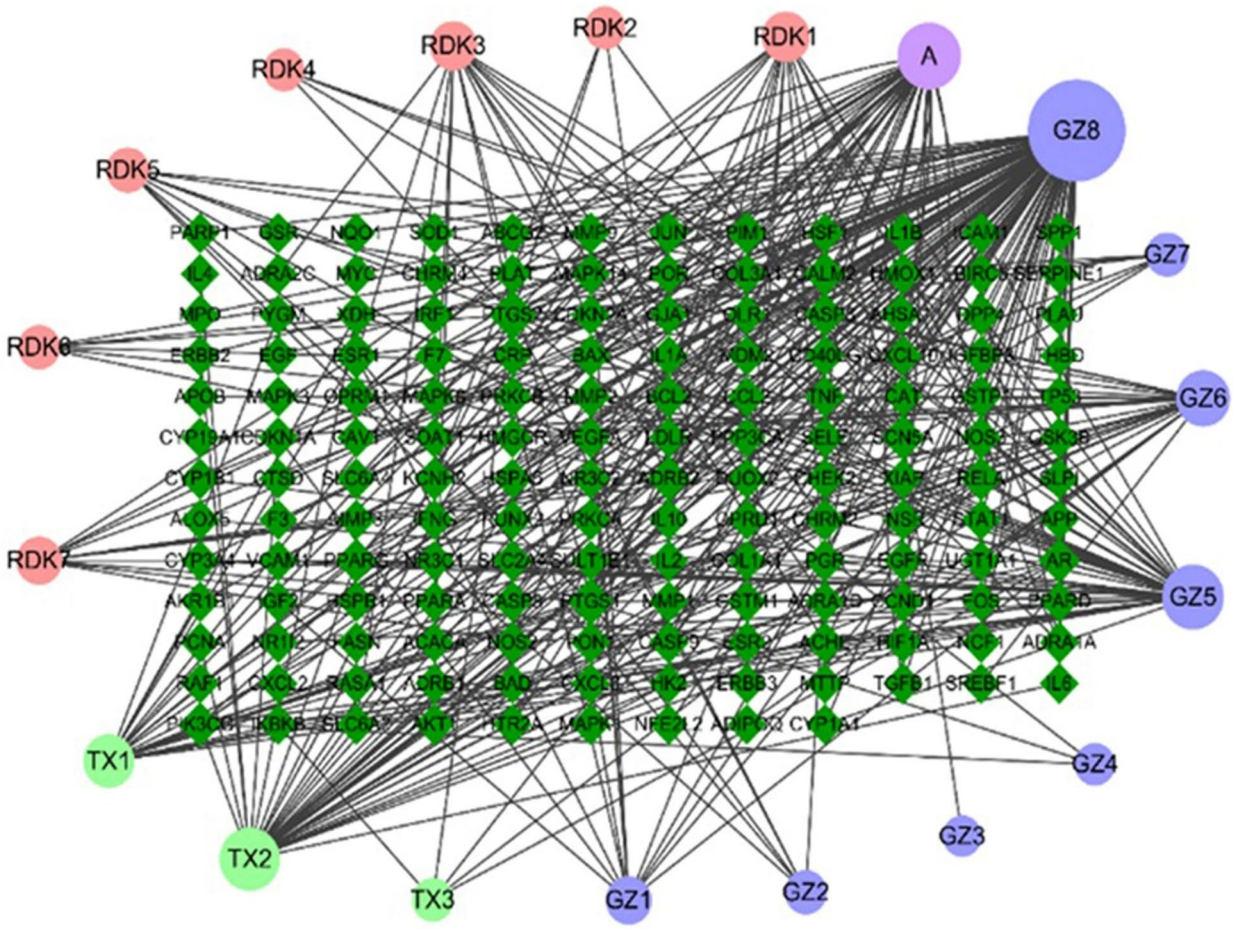


Fig. 1 Drug–component–target network of Mongolian medicine Sanwei Tanxiang Tangsan (STX). Network diagram constructed in Cytoscape 3.7.1 showing the interactions between the active components of STX and the common targets related to heart failure. Green diamonds represent the intersecting target genes. Light green nodes (TX1–TX3) denote active components from *Santalum album*, blue nodes (GZ1–GZ8) denote components from *Choerospondias axillaris*, and red nodes (RDK1–RDK7) denote components from *Myristica fragrans*. The purple node (**A**) represents β-sitosterol, the shared component between *Choerospondias axillaris* and *Myristica fragrans*. The density of edges reflects the complexity of interactions between components and targets. This network represents predicted interactions based on database-derived information and does not imply direct biological validation

disease networks and should be interpreted cautiously as potential rather than disease-specific targets.

GO analysis and KEGG pathway analysis

Annotation results obtained from the DAVID database included 741 entries for BP, primarily associated with the positive regulation of gene expression, apoptotic processes and their inhibition, and cellular responses to exogenous stimuli; 81 entries for CC, mainly related to the endosomal lumen, perinuclear cytoplasmic region, extracellular space, and transcription regulator complex; and 137 entries for MF, predominantly involving protein binding, enzyme binding, protein homodimerization activity, oxidoreductase activity, steroid binding, and transcription coactivator binding (Fig. 3). Additionally, 179 KEGG pathways were identified, among which representative disease-related pathways included the AGE/RAGE signaling pathway, lipid and atherosclerosis, pathways in cancer, fluid shear stress and atherosclerosis, IL-17 signaling pathway, TNF signaling pathway, endocrine resistance, and HIF-1 signaling pathway (Fig. 4). These enrichment results provide a broad overview of potential biological processes and pathways but do not establish direct causal relationships.

Molecular docking

Molecular docking and visualization analyses were conducted using AutoDockTools 1.5.6 software for the top five core target proteins ranked by degree value (AKT1, IL1B, TP53, TNF, and IL6) and their corresponding active components (quercetin, kaempferol, luteolin, naringenin, and isorhamnetin). The docking outcomes are summarized in Table 2. The results indicated that all molecular complexes exhibited binding energies below −5.5 kcal/mol, suggesting that the active components possessed moderate predicted binding affinities toward

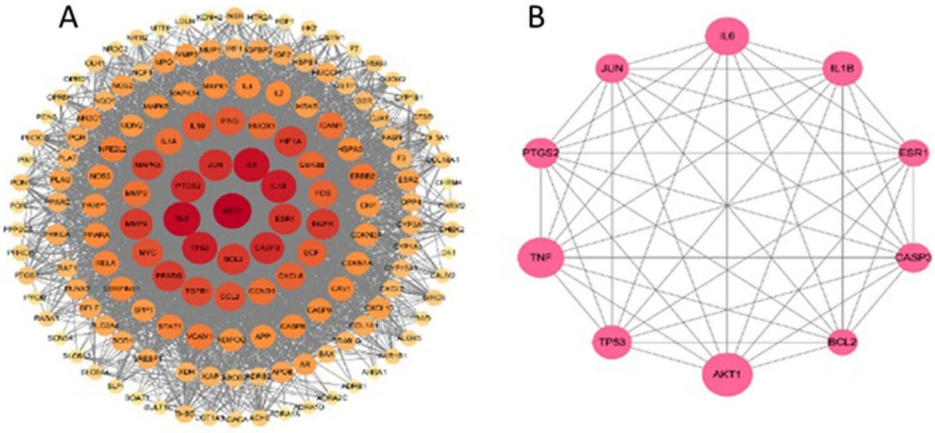


Fig. 2 Protein–protein interaction (PPI) network and core hub genes of the common targets of STX in heart failure. (**A**) Global PPI network of the 153 overlapping targets obtained from the STRING database (confidence score ≥ 0.4) and visualized in Cytoscape 3.7.1. Node color depth from yellow to dark red indicates increasing degree value (number of interactions). (**B**) Subnetwork of the top hub genes screened by degree value, including AKT1, TP53, TNF, IL6, IL1B, PTGS2, CASP3, ESR1, JUN, and BCL2, illustrating the close connectivity among core regulatory targets. These hub genes are identified based on network topology and may represent general regulatory nodes rather than disease-specific targets

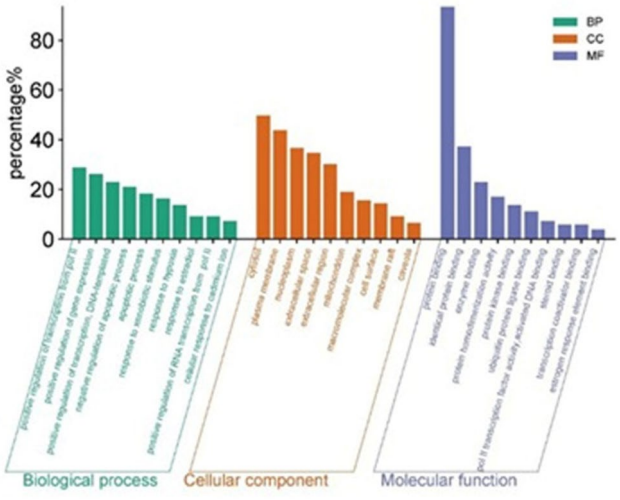


Fig. 3 Gene Ontology (GO) enrichment analysis of the common targets of STX and heart failure. Bar chart displaying the top enriched GO terms in three categories: biological process (BP, green), cellular component (CC, orange), and molecular function (MF, blue). The x-axis shows representative GO terms, and the y-axis indicates the percentage of genes annotated to each term. The results highlight enrichment in processes related to regulation of gene expression, apoptosis, response to external stimuli, endosomal and perinuclear localization, and protein binding–related functions. These enrichment results reflect functional associations and do not establish direct mechanistic relationships

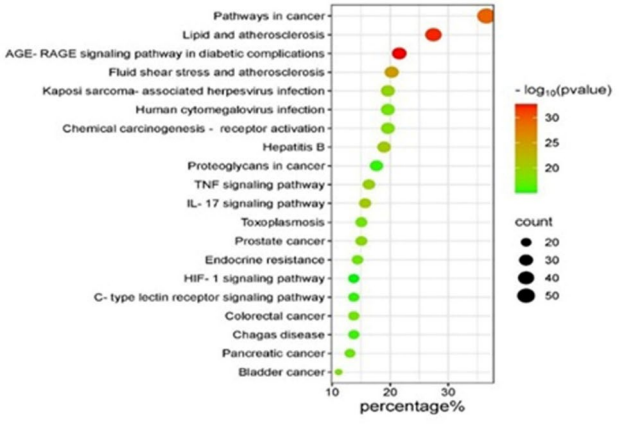


Fig. 4 KEGG pathway enrichment analysis of the common targets of STX in heart failure. Bubble plot of the top enriched KEGG pathways. The x-axis represents the percentage of genes involved in each pathway, and bubble size reflects the gene count. The color scale corresponds to –log10(P value), with warmer colors indicating higher statistical significance. Enriched pathways include "Pathways in cancer", "Lipid and atherosclerosis", "AGE–RAGE signaling pathway in diabetic complications", "Fluid shear stress and atherosclerosis", TNF and IL-17 signaling pathways, HIF-1 signaling, and other inflammation- and apoptosis-related pathways. These pathways are derived from enrichment analysis and should be interpreted as potential biological associations rather than confirmed signaling mechanisms

their respective target proteins, among which the AKT1–luteolin complex displayed the most stable interaction. Furthermore, PyMOL software was employed to visualize the docking conformations of AKT1, IL6, and TP53 with their respective ligands, all exhibiting binding energies below −5.85 kcal/mol. The primary docking diagrams and their corresponding magnified detail views clearly illustrated the specific amino acid binding sites and hydrogen-bond interactions between the small-molecule ligands and receptor proteins. These findings are based on computational predictions and require further experimental validation.

Effects of Mongolian medicine STX on the degree of HF in rats

Serum NT-proBNP measurements revealed that compared with the Con group, NT-proBNP levels in the Mod group were markedly elevated. In contrast, both the STX

Table 2 Binding energy of key targets and key components. Binding energies were predicted using AutoDockTools 1.5.6, with lower values indicating stronger predicted binding affinity

Symbol	PDB ID	Molecule name	MOL ID	Binding energy (kcal/mol)
AKT1	6npz	Quercetin	MOL000098	−6.61
		Naringenin	MOL004328	−6.57
		Kaempferol	MOL000422	−6.60
		Luteolin	MOL000006	−7.63
TNF	1ca4	Quercetin	MOL000098	−5.70
		Kaempferol	MOL000422	−5.59
		Luteolin	MOL000006	−5.53
IL6	1alu	Quercetin	MOL000098	−5.85
		Luteolin	MOL000006	−6.44
IL1β	1t4q	Quercetin	MOL000098	−6.68
TP53	8dc6	Quercetin	MOL000098	−6.52
		Luteolin	MOL000006	−6.69

and ARNI groups exhibited significantly reduced NT-proBNP levels relative to the Mod group. Cardiac echocardiographic analysis (Fig. 5) indicated that, compared with the Control group, the Model group showed significant alterations in ejection fraction, fractional shortening, and left ventricular end-systolic diameter (Fig. 5A and B). However, no statistically significant differences were observed between the STX or ARNI groups and the Model group (Fig. 5B, C). Although slight numerical improvements in EF and FS were observed, these changes did not reach statistical significance, indicating that functional recovery was not conclusively demonstrated by echocardiographic parameters under the present experimental conditions. The detailed information is summarized in Table 3.

Detection of AKT1, IL6, and P53 content in tissues by ELISA

ELISA analysis of myocardial tissues revealed that compared with the Con group, AKT1 levels in the Mod group were markedly diminished, whereas IL6 and P53 levels were markedly elevated. In comparison with the Mod group, AKT1 levels in the STX and ARNI groups were markedly increased, with a more pronounced elevation observed in the STX group. Conversely, IL-6 and p53 protein levels showed a decreasing trend following STX and ARNI treatment. These results reflect changes in total protein abundance and do not directly indicate activation status of the corresponding signaling pathways. The detailed information is summarized in Table 3.

Masson staining results

In the Masson-stained sections (Fig. 6), collagen fibers were distinctly stained blue, whereas muscle fibers and

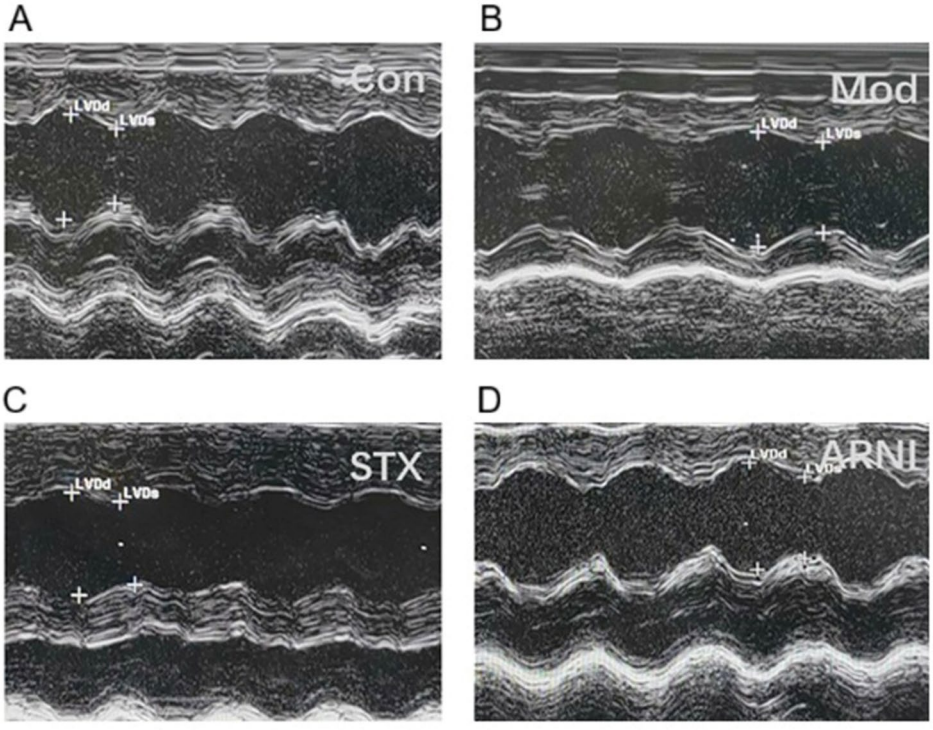


Fig. 5 Representative echocardiographic M-mode images of left ventricular function in each experimental group. (**A**) Control (Con) group. (**B**) Doxorubicin-induced heart failure model (Mod) group. (**C**) Mongolian medicine Sanwei Tanxiang Tangsan (STX) treatment group. (**D**) Sacubitril/valsartan (ARNI) treatment group. LVDd and LVDs indicate left ventricular end-diastolic and end-systolic diameters, respectively. These images correspond to the quantitative echocardiographic parameters summarized in Table 3. Although representative images are shown, no statistically significant differences in EF and FS were observed between the STX or ARNI groups and the Model group

Table 3 Comparison of cardiac function parameters and NT-proBNP levels in rat groups

Group	FS (%)	EF (%)	LVDd (mm)	LVDs (mm)	NT-proBNP (pg/mL)
Con	49.63 ± 9.23	84.88 ± 7.24	5.40 ± 0.48	2.75 ± 0.59	35.59 ± 2.31
Mod	24.50 ± 4.50**	54.50 ± 7.63**	5.20 ± 0.45	3.91 ± 0.34**	53.74 ± 0.86**
STX	25.75 ± 4.62	56.50 ± 7.43	5.08 ± 0.40	3.80 ± 0.43	50.66 ± 2.66▲▲
ARNI	26.38 ± 4.53	57.75 ± 7.38	5.50 ± 0.39	4.06 ± 0.43	45.36 ± 0.98▲▲

Note: $n = 8$. Data are expressed as mean ± standard deviation ($\bar{x} \pm s$)

*$P < 0.05$ and **$P < 0.01$ vs. Con group; ▲ $P < 0.05$ and ▲▲ $P < 0.01$ vs. Mod group. Values without symbols indicate no statistically significant difference. No statistically significant differences were observed in FS, EF, LVDd, or LVDs between the STX/ARNI groups and the Mod group. The relatively high EF values in the Con group may reflect variability inherent to small-animal echocardiographic measurements.*

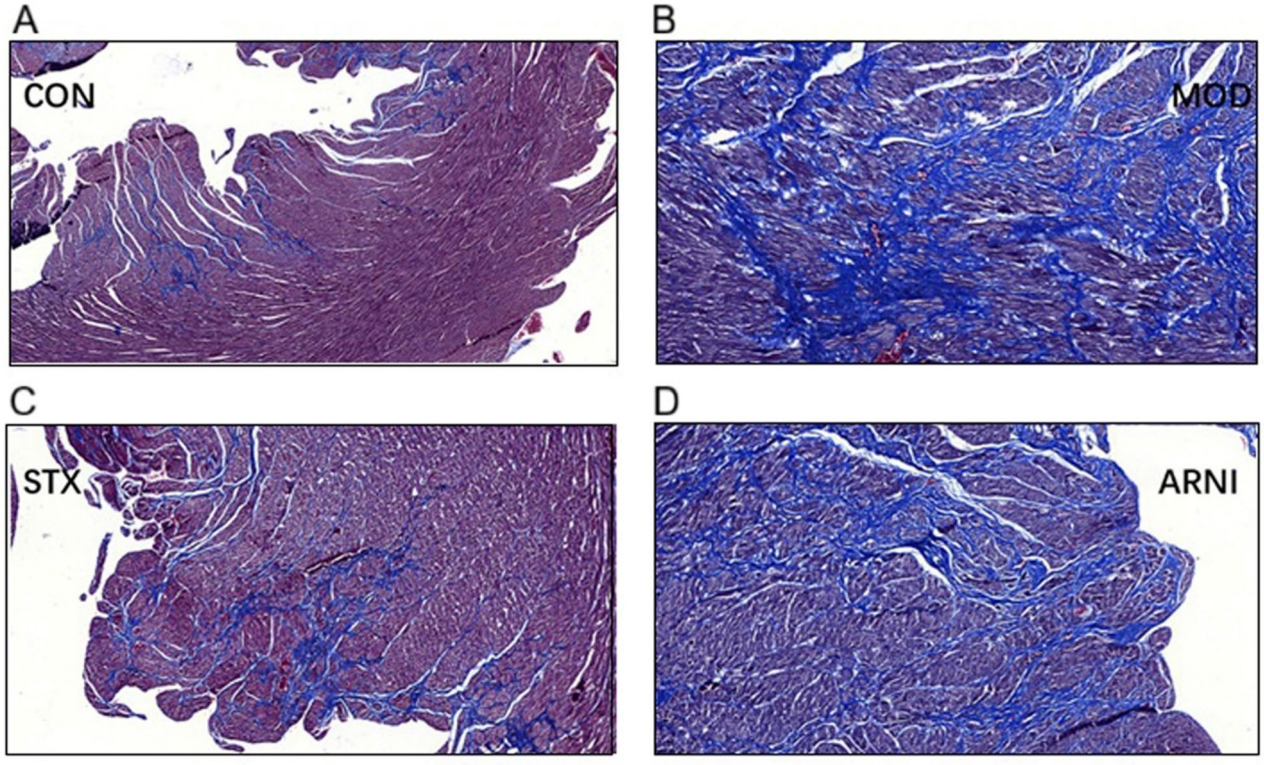


Fig. 6 Masson's trichrome staining of myocardial tissue in each experimental group. Representative myocardial sections stained with Masson's trichrome (collagen fibers in blue, muscle fibers in red) from (**A**) Control (Con) group, (**B**) Model (Mod) group, (**C**) STX group, and (**D**) ARNI group (original magnification ×400). The Mod group shows extensive blue collagen deposition and disrupted myocardial architecture, indicating severe myocardial fibrosis. Both STX and ARNI treatment groups exhibit reduced collagen fiber accumulation and improved myocardial structural integrity compared with the Mod group. These observations are qualitative, as quantitative assessment of fibrosis was not performed

other tissues appeared red. Microscopic observations revealed that, compared with the Control group, the Model group exhibited a substantial increase in blue-stained collagen fibers within the myocardial tissue, accompanied by a widespread distribution (Fig. 6A and B). The originally continuous red muscle fiber regions were extensively disrupted and segmented by dense blue collagen fibers, indicating markedly aggravated myocardial fibrosis in the Model group. In comparison with the Model group, both the STX and ARNI treatment groups displayed a pronounced reduction in blue collagen fibers within the myocardial tissue, along with an evident expansion of red muscle fiber areas (Fig. 6C and D). These results suggest that both STX and ARNI interventions effectively mitigated myocardial fibrosis and improved the pathological morphology of myocardial tissue. However, fibrosis was not quantitatively assessed, and these observations remain qualitative.

Discussion

In Mongolian medicine, "Qi (Heyi) stagnation and blood stasis" are regarded as the fundamental pathogenesis of HF [6]. The pathological essence is reflected in the impaired circulation of Heyi and Qisu (disturbed blood flow), which consequently disrupts the normal metabolism of Qi, blood, and body fluids, ultimately leading to cardiac dysfunction [7]. The Mongolian medicine STX exhibits potential therapeutic efficacy in HF through an

integrative regulatory mechanism of "regulating Heyi, promoting Qi and blood circulation, and eliminating water-dampness" [8]. Numerous studies have demonstrated that this formulation possesses distinctive advantages in the clinical management of cardiovascular diseases [9].

Cardiac remodeling constitutes a major pathogenic mechanism underlying HF, with myocardial fibrosis serving as the predominant manifestation of structural remodeling. This process is characterized by excessive collagen fiber accumulation within myocardial tissue and the destruction of normal myocardial architecture. The onset and progression of HF-induced myocardial fibrosis are closely related to inflammatory responses [10] and apoptosis [11]. These factors together establish a self-perpetuating cycle of "inflammatory activation–apoptosis–fibrosis exacerbation", ultimately leading to irreversible cardiac dysfunction.

The AKT1/P53 signaling pathway regulates myocardial injury through modulation of multiple effector proteins [12]. Protein kinase B (AKT) functions as a key intracellular serine/threonine kinase widely distributed among various tissues and cells. Among its isoforms, AKT1 exhibits the broadest distribution across different tissues and acts as a central molecule in regulating both physiological and pathological processes within the cardiovascular system [13]. Previous studies have shown that transient activation of AKT1 preserves cardiac homeostasis through multiple mechanisms, including the promotion of coronary angiogenesis, inhibition of cardiomyocyte apoptosis and oxidative stress, regulation of metabolism and inflammatory signaling, restoration of myocardial energy supply, maintenance of myocardial contractility, and suppression of ventricular remodeling [14–16].

In the AKT-mediated cardiovascular protective mechanism, the regulatory interplay between AKT and the tumor suppressor gene p53 constitutes a central component. As a downstream effector of AKT, the activity and expression of p53 are directly governed by the phosphorylation status of AKT. Once activated, phosphorylated AKT suppresses the aberrant activation of p53 through either direct interaction or indirect modulation of related molecular pathways [17]. Under stress conditions such as myocardial ischemia and inflammation, p53 becomes activated and induces an imbalance in Bcl-2 family proteins via the mitochondrial pathway, resulting in decreased mitochondrial membrane potential and cytochrome C release, thereby initiating the intrinsic apoptotic cascade. Moreover, p53 can also promote apoptosis by activating downstream molecules through the death receptor pathway, mediating extrinsic apoptotic signaling [18]. Extensive cardiomyocyte apoptosis directly impairs myocardial contractility, accelerates ventricular remodeling, and promotes the progression of HF.

Notably, a bidirectional regulatory interaction exists between the AKT/p53 signaling pathway and inflammatory responses, with IL-6 functioning as an essential molecular bridge linking the two. As a principal mediator of inflammatory activity, elevated IL-6 levels intensify local cardiovascular inflammation and increase vascular permeability, thereby heightening the risk of cardiovascular events [19]. Concurrently, p53 facilitates the release of pro-inflammatory mediators such as IL-6 by regulating the transcription of inflammation-associated genes, further amplifying tissue inflammatory injury and inducing cellular apoptosis [20]. Upon phosphorylation, AKT suppresses p53 activity directly, thereby diminishing its role in mediating pro-inflammatory gene transcription. Similarly, AKT can also reduce IL-6 secretion by modulating key molecules involved in inflammatory signaling cascades [21].

Considering these regulatory mechanisms of the AKT/p53 signaling pathway in cardiac pathology, together with the findings from this investigation of Mongolian medicine STX, a central mechanistic hypothesis is proposed: Mongolian medicine STX may exert myocardial protective effects that are associated with modulation of AKT1/p53-related signaling, although direct pathway activation was not confirmed in the present study.

The primary active constituents of Mongolian medicine STX are quercetin, kaempferol, naringenin, and luteolin, all of which belong to the flavonoid class. As natural antioxidants, flavonoids scavenge reactive oxygen species (ROS) and exert antioxidant, anti-inflammatory [22], cytoskeletal-stabilizing, and ferroptosis-inhibitory effects [23], thereby conferring cardioprotective benefits. Quercetin enhances myocardial antioxidant defense by eliminating free radicals and activating superoxide dismutase, while inhibiting mitochondrial apoptosis through the upregulation of anti-apoptotic proteins (e.g., B-cell lymphoma factor 2, Bcl-2) and suppression of pro-apoptotic proteins (e.g., B-cell lymphoma factor 2-associated X protein) [24]. Kaempferol mitigates mitochondrial ROS accumulation and regulates calcium homeostasis to prevent calcium overload injury [25], simultaneously attenuating cardiomyocyte apoptosis, inflammation, and hypoxic damage [26]. Naringenin improves myocardial energy metabolism disrupted by ischemia and suppresses inflammatory factor release via the PI3K/Akt/eNOS pathway, thereby preventing cardiomyocyte necrosis and apoptosis [27]. Luteolin decreases ROS and malondialdehyde levels, downregulates ferroptosis markers Acsl4 and Ptgs2, and inhibits Bax and p53 expression through the Akt/P53/Mdm2 signaling pathway, ultimately enhancing myocardial contractility.

Myocardial fibrosis is a pathological condition characterized by excessive collagen fiber deposition within myocardial tissue and disruption of the normal myocardial

architecture. Its onset and progression are tightly linked to inflammation and apoptosis, forming a self-perpetuating cycle of "inflammatory activation–cellular apoptosis–fibrosis exacerbation" that culminates in irreversible cardiac dysfunction.

The results of this study indicated that the doxorubicin-induced HF rat model displayed typical pathological features of HF, including markedly elevated NT-proBNP levels and abnormal echocardiographic parameters. After intervention with Mongolian medicine STX, NT-proBNP levels were significantly reduced; however, echocardiographic parameters (EF and FS) showed only slight numerical improvement without statistical significance, indicating that functional recovery was not conclusively demonstrated. The expression of AKT1 protein in myocardial tissue was markedly upregulated in the Mongolian medicine STX group, suggesting a potential association with activation of AKT1-related signaling pathways. However, as only total protein levels were measured, pathway activation could not be directly confirmed. IL-6 levels in myocardial tissue were markedly decreased, indicating a reduction in inflammatory mediator levels rather than direct inhibition of specific pathways such as NF-κB. Similarly, P53 protein levels were markedly reduced, reflecting decreased total protein abundance; however, phosphorylation status and downstream apoptotic signaling were not evaluated in this study. These experimental findings were partially consistent with the predictions of network pharmacology analysis, although such computational predictions require further experimental validation. From the perspective of Mongolian medical theory, Qi stagnation and blood stasis represent major pathological mechanisms underlying HF, primarily manifested as impaired blood circulation and insufficient myocardial blood and oxygen supply, ultimately resulting in reduced cardiac function. Mongolian medicine STX may ameliorate the state of Qi stagnation and blood stasis through multiple mechanisms, potentially involving improvement of myocardial microcirculation, attenuation of inflammatory responses, and reduction of cardiomyocyte apoptosis. Concurrently, reduction of IL-6 expression may contribute to decreased inflammatory injury and improved vascular function. Meanwhile, downregulation of P53 may be associated with reduced cardiomyocyte apoptosis, thereby helping to maintain both structural and functional cardiac integrity.

However, several limitations should be acknowledged. First, AKT1 and p53 were assessed only at the total protein level using ELISA, and phosphorylation-dependent activation of the signaling pathway was not evaluated. Second, key downstream apoptotic markers such as BAX, BCL2, and caspase-3 were not measured. Third, echocardiographic parameters did not show statistically significant improvement, indicating limited functional recovery under the present experimental conditions. Fourth, myocardial fibrosis was evaluated qualitatively without quantitative analysis. Finally, the doxorubicin-induced model primarily reflects cardiotoxic injury and may not fully represent other forms of heart failure. Future studies should incorporate more comprehensive mechanistic experiments, including assessment of phosphorylated proteins, apoptosis markers, and additional HF models, to further validate these findings.

Conclusion

In conclusion, this study suggests that Mongolian medicine STX may ameliorate myocardial pathological alterations and partially improve biochemical indicators associated with heart failure, as evidenced by reduced NT-proBNP levels and improved histological features. The findings from network pharmacology and experimental analysis indicate that these effects may be associated with AKT1/p53-related signaling pathways, although direct pathway activation and causal mechanisms were not confirmed in the present study. Therefore, these results provide a preliminary theoretical basis for the potential application of Mongolian medicine STX in HF, and further mechanistic and functional studies are required to validate these observations.

Supplementary Information

The online version contains supplementary material available at https://doi.org/10.1186/s13019-026-04362-9.

Supplementary Material 1

Acknowledgements

We are grateful to the staff of the Laboratory Animal Center of Inner Mongolia Medical University for their assistance with animal care and technical support. We also thank our colleagues in the Department of Mongolian Medicine for their helpful discussions during the course of this work.

Author contributions

ARuNa (AR), Dulan (DL), and GuiZhi (GZ) gathered data and analyzed and interpreted it. AR and DL performed the network pharmacology and molecular docking analyses. AR and GZ carried out the animal experiments. AR and Hua Li (HL) conceptualized and designed the research. HL supervised this work, gave critical comments on the research, revised the intellectual content, and edited the final manuscript. Davaadagva Damdinjav (DD) and Battulga Tungalag (BT) contributed to data interpretation and manuscript revision. All authors read and agreed to the published version of the manuscript.

Funding

This work was supported by the Inner Mongolia Natural Science Foundation Project (2020MS08050), the Inner Mongolia Health Science and Technology Plan Project (202201210), the Research Project of Inner Mongolia Autonomous Region Mongolian Medicine Collaborative Innovation Center (MYYXTPY202305), the International Cooperation Guidance Project of Inner Mongolia Autonomous Region Mongolian Medicine Collaborative Innovation Center (MYYXTGJ202401), the "First-Class Discipline" Science and Technology Cooperation Project of Traditional Chinese Medicine at Inner Mongolia Medical University (International Cooperation Project) (2025MYXYLXK005) and Inner Mongolia Natural Science Foundation (2024QN08035).

Data availability
Data related to this study are provided within the manuscript. Additional raw data are available from the corresponding author upon reasonable request.

Declarations

Ethics approval and consent to publication
The Laboratory Animal Welfare and Ethics Committee of Inner Mongolia Medical University approved the study protocol and assigned the ethical number KYD20240386. All procedures involving animals were conducted in accordance with institutional and international guidelines for the care and use of laboratory animals.

Consent for publication
Not applicable.

Competing interests
The authors declare no competing interests.

Received: 6 February 2026 / Accepted: 28 May 2026
Published online: 10 June 2026

References

1. Heidenreich PA, Bozkurt B, Aguilar D, et al. 2022 AHA/ACC/HFSA guideline for the management of heart failure: a report of the American College of Cardiology/American Heart Association Joint Committee on Clinical Practice Guidelines [J]. Circulation. 2022;145(18):895–1032.
2. McDonagh TA, Metra M, Adamo M, et al. 2021 ESC guidelines for the diagnosis and treatment of acute and chronic heart failure: developed by the Task Force for the Diagnosis and Treatment of Acute and Chronic Heart Failure of the European Society of Cardiology (ESC) with the special contribution of the Heart Failure Association (HFA) of the ESC [J]. Eur Heart J. 2021;42(36):3599–726.
3. Jinghong Luo. Mechanism of hydrochlorothiazide in improving cardiac remodeling in rats with heart failure after myocardial infarction by alleviating myocardial oxidative stress [D]. Southern Medical University; 2025. p. 88.
4. Wu R. Nashundala, Xin Ming. Research overview of Mongolian medicine in treating chronic heart failure [J]. J Med Pharm Chin Minorities. 2022;28(8):67–9.
5. Sun YH, Bu R, Wang YW, et al. Validation of efficacy and mechanism of Sanwei-Tanxiang powder in improving myocardial ischemia reperfusion injuries. Sci Rep. 2021;11(1):664.
6. Li F, Li H, Meng Y. Literature research on the distribution patterns of Mongolian medicine syndrome types, symptoms, and signs in chronic heart failure. Journal of Inner Mongolia Medical University. 2023;45(3):250–2.
7. Xin Ming. Study on the effect of Mongolian medicine Ganlu Yangxin Pills on urine volume and rehospitalization rate in Jiruhen Habeng disease [D]. Inner Mongolia Med Univ, 2023: 42.
8. Mei Yang Y, Li Q, Yu, et al. Effect of Sanwei Tanxiang San on improving right ventricular remodeling in rats with high-altitude pulmonary hypertension [J]. West China J Pharm Sci. 2017;32(6):579–82.
9. Li H, Li HF, et al. Meta-analysis of efficacy and safety of Mongolian medicine Zandan-3 Decoction in treating coronary heart disease angina pectoris [J]. J Inner Mongolia Med Univ. 2022;44(3):243–7.
10. Li S, Yang M, Zhao Y, et al. Deletion of ASPP1 in myofibroblasts alleviates myocardial fibrosis by reducing p53 degradation [J]. Nat Commun. 2024;15(1):8425.
11. Alexanian M, Padmanabhan A, Nishino T, et al. Chromatin remodelling drives immune cell–fibroblast communication in heart failure. Nature. 2024;635(8038):434–43.
12. Chen L, Chen LJ, Shen HW, et al. Inhibition of HIF-2α expression in cardiomyocytes attenuates PCB126-induced cardiotoxicity associated with decreased apoptosis through the PI3K/Akt and p53 signaling pathways. Ecotoxicol Environ Saf. 2024;286:117185.
13. Degan S, Gelman I. Emerging roles for AKT isoform preference in cancer progression pathways. Mol Cancer Res. 2021;19(8):1251–7.
14. Fang Z, Wei W, Jiang X. Monotropein attenuates doxorubicin-induced oxidative stress, inflammation, and arrhythmia via the AKT signal pathway. Biochem Biophys Res Commun. 2023;638:14–22.
15. Zhang G, Sun X, Yu K, et al. Improvement of ventricular remodeling and regulation of PI3K/Akt/mTOR signaling pathway in rats with heart failure by polysaccharides from Stropharia rugosoannulata [J]. Volume 20. Molecular & Cellular Toxicology; 2024. pp. 521–31. 3.
16. Zhang Z, Wu Y, Chen K, et al. Exploring the intervention mechanism of Yiqi Fumai Formula on experimental heart failure mice based on the heart-gut axis [J]. China J Chin Materia Med. 2025;50(12):3399–412.
17. Popova NV, Jücker M. The role of mTOR signaling as a therapeutic target in cancer. Int J Mol Sci. 2021;22:1743.
18. Zheng N, Li H, Wang X, et al. Oxidative stress-induced cardiomyocyte apoptosis is associated with dysregulated Akt/p53 signaling pathway. J Recept Signal Transduct. 2020;40(6):599–604.
19. Mehta N, de Goma E, Shapiro MD. IL-6 and cardiovascular risk: a narrative review. Curr Atheroscler Rep. 2024;27(1):12.
20. Fei X, Chen L, Gao J, et al. p53 lysine-lactylated modification contributes to lipopolysaccharide-induced proinflammatory activation in BV2 cells under hypoxic conditions [J]. Neurochem Int. 2024;178:105794.
21. Zhao F, Wen W, Xuejun J. Monotropein attenuates doxorubicin-induced oxidative stress, inflammation, and arrhythmia via the AKT signal pathway. Biochem Biophys Res Commun. 2023;638:14–22.
22. Zhang K, Liu C, Yang K. Flavonoids ameliorate ferroptotic cell death in cardiomyocytes through ROS scavenging and lipid peroxide reduction. FASEB J. 2022;36(S1):fasebj.2022.36.S1.0R522.
23. Liu DL, Liu SJ, Hu SQ, et al. Probing the potential mechanism of quercetin and kaempferol against heat stress-induced Sertoli cell injury: through integrating network pharmacology and experimental validation. Int J Mol Sci. 2022;23(19):11163.
24. Xiong D, Wang X, Wang H, et al. Quercetin inhibits cardiomyocyte apoptosis via Sirt3/SOD2/mitochondrial reactive oxygen species during myocardial ischemia–reperfusion injury. Heliyon. 2024;10(21):e39031.
25. Kamisah Y, Jalil J, Yunos NM, et al. Cardioprotective properties of kaempferol: a review. Plants Basel. 2023;12(11):2096.
26. Hagiwara H, Watanabe M, Fujioka Y, et al. Stimulation of the mitochondrial calcium uniporter mitigates chronic heart failure-associated ventricular arrhythmia in mice. Heart Rhythm. 2022;19(10):1725–35.
27. Zheng M, Gou H, Zi C et al. Naringenin ameliorates myocardial ischemia-reperfusion injury in rats by regulating the PI3K/Akt/eNOS pathway [J]. Liaoning J Traditional Chin Med, 2025: 1–12.

Publisher's note

Springer Nature remains neutral with regard to jurisdictional claims in published maps and institutional affiliations.